ELSEVIER

Thermochimica Acta 266 (1995) 65–77

thermochimica acta

Calorimetric and DTA studies of 1,3-dioxolane hydrate and (1,3-dioxolane)$_{1-x}$ (tetrahydrofuran)$_x$ mixed hydrates ☆,α

Tadashi Yonekura [1], Osamu Yamamuro, Takasuke Matsuo *, Hiroshi Suga [2]

Department of Chemistry and Microcalorimetry Research Center, Faculty of Science, Osaka University, Toyonaka, Osaka 560, Japan

Abstract

The heat capacities of 1,3-dioxolane clathrate hydrates (DXL·17H_2O) doped with potassium hydroxide ($x = 1.8 \times 10^{-4}$ and 1.8×10^{-3} to water) were measured with an adiabatic calorimeter in the temperature range between 13 and 300 K. A glass transition due to freezing of the water reorientation appeared at 43 K in both samples. The relaxation time of the reorientational motion of the water molecule was obtained from the enthalpy relaxation data and the corresponding activation enthalpy was determined to be about 8 kJ mol^{-1} for both samples. A eutectic melting between DXL hydrate and KOH hydrate occurred at 216 K in the sample richer in KOH ($x = 1.8 \times 10^{-3}$), indicating that the solubility limit of KOH to DXL hydrate is around $x = 1.8 \times 10^{-4}$. Differential thermal analyses of (1,3-dioxolane)$_{1-x}$(tetrahydrofuran)$_x$ mixed hydrates doped with KOH ($x = 1.8 \times 10^{-4}$) were performed in the temperature range between 20 and 100 K. The transition temperature reported in tetrahydrofuran hydrate ($T_{trs} = 62$ K) decreased with increase in x and the transition did not occur for $x < 0.6$ owing to the slowing down of the transition rate. This result indicates that the ordering transition of the water and guest molecules did not occur in DXL hydrate because the hypothetical transition temperature is lower than the freezing temperature of the water reorientation.

Keywords: Calorimetry; Dioxolane clathrate hydrates; DTA; Heat capacity; Transition

* Corresponding author.

☆ Dedicated to Hiroshi Suga on the Occassion of his 65th Birthday.

α Contribution No. 106 from the Microcalorimetry Research Center.

[1] Present address: Osaka Mint Bureau, Ministry of Finance, Temma, Kita-ku, Osaka 530, Japan.

[2] Present address: Research Institute for Science and Technology, Kinki University, Kowakae, Higashi-Osaka 577, Japan.

SSDI 0040-6031(95)02452-2

1. Introduction

Clathrate hydrates [1–5] are well-known inclusion compounds occurring in nature. The host lattice is made of water molecules, forming a three-dimensional hydrogen-bonded network similar to those of various ice polymorphs. The guest molecules are accommodated in the well-defined cages of the host lattice by van der Waals interaction. More than 100 guest molecules have been known to be enclathrated so far in the six types of host lattice, depending on their sizes and shapes; most of them are enclathrated in structure **I** and **II** host lattices. 1,3-Dioxolane (DXL) and tetrahydrofuran (THF) form structure **II** hydrates. The unit cell of the structure **II** host lattice is composed of two pentagonal dodecahedral and eight tetrakaidecahedral cages formed by 136 water molecules. The guest molecules are enclathrated only in the hexakaidecahedral cages and so the composition is stoichiometrically $M \cdot 17H_2O$ (M is the guest molecule).

One of the interesting aspects of the clathrate hydrates is the orientational disorder which both the guest and host species exhibit. Orientational disorder in crystals is usually removed through one or more phase transitions at low temperatures. In all the clathrate hydrates, however, the orientational disorder of the water molecules is believed to be frozen-in before the crystal reaches its hypothetical ordering transition on cooling. Actually, a glass transition due to a slowing down of the water reorientational motion was observed by adiabatic calorimetry in structure **I** ethylene oxide hydrate (80 K) [6], structure **I** and **II** trimethylene oxide hydrate (90 K) [7, 8], structure **II** THF hydrate (85 K) [9], and structure **II** acetone hydrate (90 K) [10]. The ordering transition of the guest molecules has only been observed for structure **I** TMO hydrate [7, 8, 11].

In our heat capacity studies, a phase transition was found to occur in THF (61.9 K) [9, 12], acetone (46.6 K) [13] and TMO (34.5 K) [8] structure **II** hydrates by doping the sample with small amounts of potassium hydroxide (KOH) ($x = 1.8 \times 10^{-4}$ to water). The transition entropies of these hydrates were about 2.5 $J\,K^{-1}\,mol^{-1}$. The dielectric measurements of these hydrates [14, 15] showed that the reorientational motion of the water molecules was accelerated drastically by doping KOH and that the water molecules were orientationally ordered at the transitions; the guest molecules were concurrently ordered in THF and acetone hydrates. A microscopic model to explain the transition entropy has not been proposed, nor has a systematic relation been found between the transition temperature and the properties of the molecules, e.g. dipole moment and van der Waals diameter.

In the present study, the heat capacity of 1,3-dioxolane (DXL) structure **II** hydrate doped with KOH was measured with an adiabatic calorimeter. DXL ($C_3H_6O_2$) molecule, which is a five-membered ring consisting of two oxygens at the 1 and 3 sites and three carbons, has a similar maximum van der Waals diameter ($d_{vdW} = 5.6$ Å) and dipole moment ($\mu = 1.46$ D) to those of THF ($d_{vdW} = 5.9$ Å and $\mu = 1.63$ D). The ordering transition was expected to occur as in the case of THF hydrate. Differential thermal analysis (DTA) of $(DXL)_{1-x}(THF)_x$ mixed hydrates doped with KOH was also performed to investigate the composition dependence of the transition temperature. Both DXL and THF molecules may be accommodated randomly in the hexa-

kaidecahedral cages since both hydrates have congruent-type phase diagrams and similar melting temperatures (DXL, 270 K; THF, 274 K) [16, 17]. The mixed hydrate should have the average properties of the transition between DXL and THF.

2. Experimental

2.1. Preparation of samples

Commercial DXL and THF reagents were purchased from Tokyo Kasei Kogyo Inc. These samples were fractionally distilled with a concentric-type rectifier HC-5500-F (Shibata Kagakukikai Kogyo Co., Ltd.). The main distillates were degassed and further distilled in vacuo in a home-made vacuum-line. No trace of organic impurity was detected by gas chromatography (Perkin-Elmer F21) in either sample. Karl–Fischer tests showed that the amount of water occluded in DXL was small enough to be neglected (0.06 mol%).

The KOH aqueous solution ($x = 1.8 \times 10^{-3}$) was purchased from Wako Pure Chemical Ind., Ltd. and used after degassing to prepare the sample solutions. Another KOH solution ($x = 1.8 \times 10^{-4}$) was prepared by diluting the above KOH solution ($x = 1.8 \times 10^{-3}$) with water purified by distillation, deionization (conductivity, 60 nS cm^{-1}) and degassing.

The sample solutions for the heat capacity measurements were prepared by mixing the above DXL liquid and KOH solutions in PTFE bottles under helium atmosphere. The compositions of the KOH-doped DXL aqueous solutions were gravimetrically determined to be DXL·16.95H_2O ($x = 1.8 \times 10^{-4}$) and DXL·16.97H_2O ($x = 1.8 \times 10^{-3}$). The (DXL–THF–water) solutions for the DTA measurements were also prepared by mixing using the gravimetric method. The mole fractions of DXL to the total guest molecules were 0, 0.1, 0.2, 0.3, 0.4 and 0.5. The composition of the KOH-doped guest aqueous solution was M·16.5H_2O ($x = 1.8 \times 10^{-4}$) (M is guest molecule) for all of the samples used for the DTA.

2.2. Heat capacity measurement

The amounts of DXL·16.95H_2O ($x = 1.8 \times 10^{-4}$) and DXL·16.97H_2O ($x = 1.8 \times 10^{-4}$) loaded in the sample cell were 10.223 g (2.6948×10^{-2} mol) and 10.560 g (2.7804×10^{-2} mol), respectively. To enhance thermal equilibration at low temperatures, the dead space of the sample cell was filled with helium gas of 9.2×10^{-5} and 7.6×10^{-5} mol, respectively.

The heat capacities of DXL·16.95H_2O ($x = 1.8 \times 10^{-4}$) and DXL·16.97H_2O ($x = 1.8 \times 10^{-4}$) were measured with an adiabatic calorimeter with a built-in refrigerator [18] in the temperature range between 13 and 300 K. The heat capacity measurement was carried out by the standard intermittent heating method, i.e. repetition of equilibration and energizing intervals. The temperature increment for each measurement was 1–2.5 K. Single-step heating experiments were performed

separately to determine the enthalpy of fusion. The accuracy of the heat capacity measurement was better than 1% at $T < 20$ K, 0.3% at $20 < T < 30$ K, and 0.1% at $T > 30$ K.

In the present calorimetry, temperature measurement was performed using a Rh–Fe resistance thermometer calibrated on the temperature scale EPT76 ($T < 30$ K) and IPTS68 ($T > 30$ K). The heat capacity difference caused by the conversion to the new temperature scale ITS90 [19] was estimated to be smaller than 0.05% over the temperature range 13–300 K.

The DXL-hydrate crystals were formed in the sample cell by cooling the sample liquids slowly (approx. 0.07 K min^{-1}). Since the DXL–water system melts congruently, the samples crystallized isothermally at about 270 K with a large exothermic effect.

2.3. *Differential thermal analysis*

The sample solutions (0.50 ± 0.01 cm^3) were placed in the home-made DTA tubes made of Pyrex glass. Helium gas was also introduced to facilitate thermal contact between the sample and DTA tube.

The DTA experiments were performed with the home-made DTA apparatus reported elsewhere [20]. The hydrate crystals were formed by cooling the sample solutions slowly (1.3 K min^{-1}). The complete formation of the mixed hydrates was checked by measuring the melting of the hydrates; a sharp endothermic peak due to the congruent melting of the mixed hydrate appeared at about 270 K. After hydrate formation, the samples were cooled down to 17 K. The cooling rate around 50 K was about 3 K min^{-1}. The DTA curves were taken in the heating direction in the temperature range between 20 and 100 K. The heating rate was about 1 K min^{-1} around 50 K for all of the DTA runs.

3. Results and discussion

3.1. *Heat capacity and congruent melting*

The observed heat capacities of DXL·$16.95H_2O$ ($x = 1.8 \times 10^{-4}$) are given in Table 1 and also plotted in Fig. 1. Two thermal anomalies were observed in the temperature range between 13 and 300 K. The first, which is our main interest, is a sudden increase in the heat capacity at 43 K. This is a glass transition due to the freezing of the reorientational motion of water. Similarities to the glass transitions of pure (KOH-undoped) clathrate hydrates [6–10] are to be noted. The ordering transition of the water molecules, which was previously observed in the KOH-doped hydrates of THF [9, 12], TMO [8], and acetone [13], did not occur in the KOH-doped DXL hydrate, even though both the size and dipole moment of the DXL molecule are similar to those of THF.

The second anomaly was the congruent melting of the DXL hydrate at 270.5 K. The enthalpy of the congruent melting was (99.6 ± 0.1) kJ mol^{-1}. This quantity

Table 1
Experimental molar heat capacities of 1,3-dioxolane clathrate hydrate (DXL·16.95H_2O) doped with KOH ($x = 1.8 \times 10^{-4}$) ($M = 379.38$ g mol^{-1}, $R = 8.31451$ J K^{-1} mol^{-1})

T/K	$C_{p,m}/R$	T/K	$C_{p,m}/R$	T/K	$C_{p,m}/R$	T/K	$C_{p,m}/R$
13.47	3.7368	50.57	29.500	105.25	41.869	201.49	65.774
13.87	3.9828	51.34	29.708	106.58	42.150	203.72	66.440
14.33	4.2606	52.11	29.911	107.91	42.474	205.95	67.121
14.82	4.5565	52.88	30.109	109.24	42.766	208.19	67.665
15.32	4.8662	53.66	30.318	110.59	43.055	210.44	68.415
15.84	5.1887	54.44	30.490	111.94	43.382	212.69	69.182
16.40	5.5464	55.23	30.677	113.30	43.661	214.94	71.444
17.00	5.9278	56.11	30.896	114.66	43.989	217.19	70.366
17.62	6.3569	57.10	31.135	116.03	44.325	219.47	71.059
18.27	6.7765	58.09	31.351	117.41	44.605	221.75	71.817
18.91	7.2136	59.09	31.593	118.79	44.915	224.04	72.601
19.56	7.6673	60.08	31.821	120.18	45.232	226.35	73.290
20.21	8.1086	61.08	32.046	121.41	45.502	228.66	74.039
20.85	8.5594	62.09	32.281	123.31	45.937	230.97	74.851
21.50	9.0047	63.09	32.500	125.21	46.385	233.30	75.686
22.15	9.4425	64.10	32.729	127.12	46.811	235.63	76.512
22.84	9.9141	65.12	32.975	129.04	47.265	237.97	77.215
23.58	10.415	66.13	33.194	130.97	47.663	240.31	78.136
24.31	10.900	67.15	33.421	132.90	48.149	242.66	79.050
25.04	11.368	68.17	33.647	134.84	48.587	245.01	79.997
25.35	11.583	69.20	33.856	136.78	49.045	247.36	80.957
26.20	12.121	70.23	34.099	138.73	49.512	249.70	81.879
27.04	12.678	71.26	34.407	140.69	49.954	252.04	83.039
27.94	13.292	72.30	34.563	142.66	50.451	254.38	84.400
28.91	14.011	73.33	34.780	144.63	50.913	256.70	86.063
29.86	14.620	74.38	35.004	146.61	51.381	259.02	88.420
30.79	15.133	75.42	35.236	148.60	51.890	261.29	92.225
31.72	15.712	76.47	35.496	150.60	52.353	263.45	97.205
32.63	16.294	77.53	35.714	152.62	52.892	265.59	105.22
33.54	16.844	78.59	35.949	154.65	53.445	267.56	132.75
34.43	17.402	79.65	36.201	156.69	53.915	269.12	227.01
35.33	17.932	80.71	36.418	158.73	54.428	269.96	449.96
36.22	18.454	81.78	36.668	160.79	54.971	270.30	1204.2
37.11	18.949	82.85	36.913	162.85	55.422	270.44	3898.1
38.01	19.427	83.92	37.139	164.93	55.970	270.47	13213
38.91	19.947	85.00	37.401	167.01	56.549	270.50	69424
39.82	20.525	86.15	37.638	169.10	57.535	270.51	75116
40.72	21.246	87.38	37.907	171.20	57.587	270.53	82432
41.59	22.102	88.61	38.202	173.31	58.184	270.60	9492.1
42.43	23.149	89.85	38.450	175.42	60.292	270.93	773.21
42.98	23.584	91.10	38.739	177.53	59.222	272.68	171.14
43.28	24.045	92.35	38.995	179.67	59.824	275.35	171.14
43.82	25.114	93.61	39.281	181.82	60.412	278.17	171.35
44.57	26.038	94.87	39.573	183.97	60.932	278.17	171.35
45.31	26.845	96.15	39.835	186.13	61.554	281.14	171.66
46.05	27.509	97.43	40.151	188.30	62.180	284.11	171.93
46.80	28.024	98.72	40.436	190.48	62.729	287.10	172.16
47.54	28.442	100.01	40.722	192.67	63.341	290.09	172.39

Table 1 (continued)

T/K	$C_{p,m}/R$	T/K	$C_{p,m}/R$	T/K	$C_{p,m}/R$	T/K	$C_{p,m}/R$
48.30	28.788	101.31	41.027	194.86	63.988	293.10	172.55
49.05	29.053	102.62	41.260	197.06	64.593	296.12	172.80
49.81	29.291	103.93	41.572	199.27	65.104	299.16	173.04

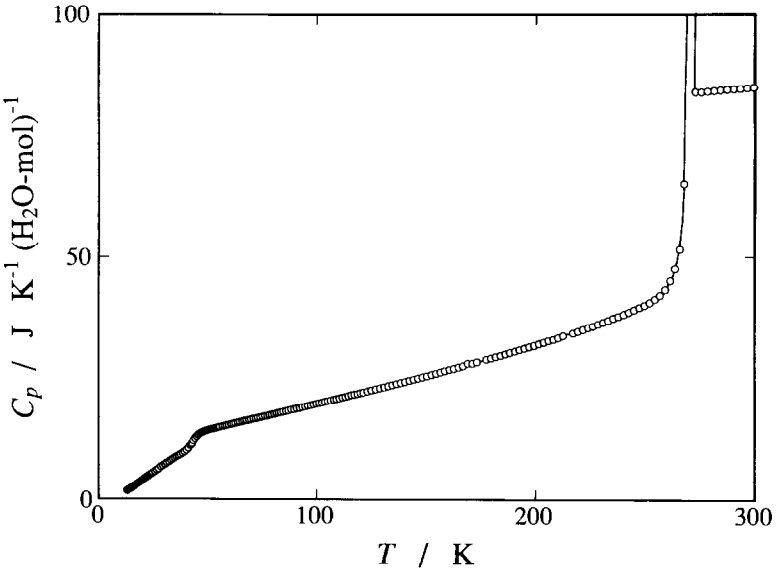

Fig. 1. Heat capacity of 1,3-dioxolane clathrate hydrate (DXL·16.95H_2O) doped with KOH ($x = 1.8 \times 10^{-4}$).

was converted to (101.4 ± 0.1) kJ mol^{-1} at the reference point (273.15 K) from the heat capacity difference between the hydrate crystal and the solution. This value was slightly larger than the value ((99 ± 1) kJ mol^{-1}) determined by Handa [17] in 1985.

3.2. Glass transition and KOH-doping effect

Fig. 2 shows the spontaneous temperature drift rate at 6 min after each energy input observed in the course of the heat capacity measurement around the glass transition. The open circles represent the data of sample A which is the DXL hydrate doped with KOH ($x = 1.8 \times 10^{-4}$), corresponding to the data in Table 1 and Fig. 1. The solid circles represent the data of sample B which is the DXL hydrate doped with KOH ($x = 1.8 \times 10^{-3}$) which is ten times more concentrated than sample A. In both samples,

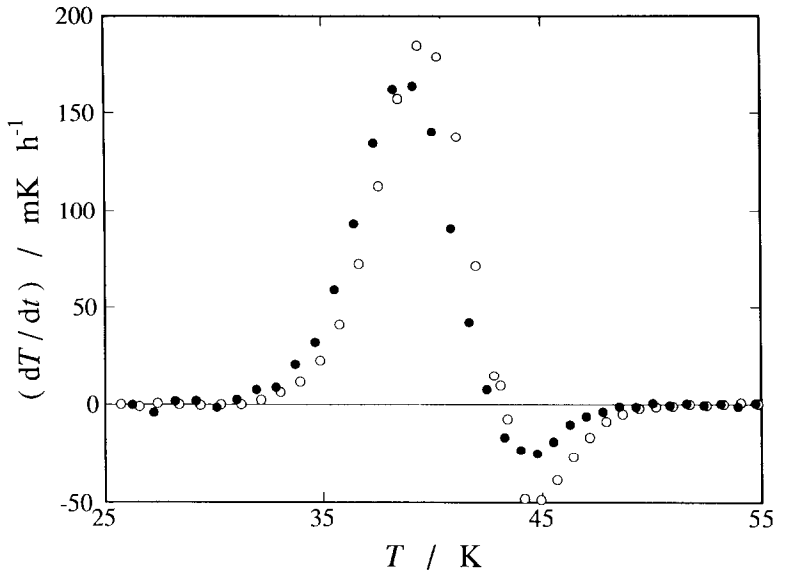

Fig. 2. Spontaneous temperature drift rates of 1,3-dioxolane hydrates doped with KOH around the glass transition: ○, sample A, DXL·16.95H_2O (KOH: $x = 1.8 \times 10^{-4}$); ●, sample B, DXL·16.97H_2O ($x = 1.8 \times 10^{-3}$).

exothermic followed by endothermic temperature drifts appeared around the temperature where the heat capacity increased abruptly. The temperature at which the drift rates went from positive to negative was the same. This temperature is the calorimetric glass transition temperature.

In the clathrate hydrates previously studied [6, 8–10], the relaxation times $\tau(T)$ related to the glass transitions could be calculated using the equation

$$d\Delta H_c(T, t)/dt = -\Delta H_c(T, t)/\tau(T)$$

where $\Delta H_c(T, t)$ and $d\Delta H_c(T, t)/dt$ are the enthalpy departure from the equilibrium state and its relaxation rate, respectively, both being determined experimentally as described elsewhere [6, 8, 9]. Using the exothermic data of both samples in Fig. 2, $\tau(T)$ of DXL hydrates doped with KOH were calculated and plotted in Fig. 3. The results of both samples were fitted well to a straight line as shown in Fig. 3. By using the Arrhenius equation

$$\tau = \tau_0 \exp(\Delta H_a/RT)$$

the activation enthalpies were calculated from the slopes of the straight lines: sample A, (8.8 ± 0.5) kJ mol^{-1}; sample B, (7.5 ± 0.5) kJ mol^{-1}. These values are close to the activation enthalpies determined from the enthalpy relaxation in KOH-doped TMO structure I hydrate (8.7 kJ mol^{-1}) [8] and the dielectric relaxations in KOH-doped THF (7.4 kJ mol^{-1}), acetone (8.5 kJ mol^{-1}) and TMO (9.0 kJ mol^{-1}) structure **II**

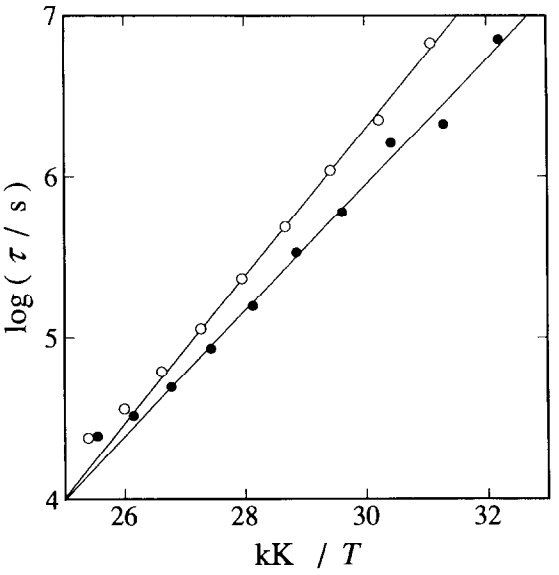

Fig. 3. Arrhenius plot of the enthalpy relaxation times of 1,3-dioxolane hydrates doped with KOH around the glass transition: ○, sample A, DXL·16.95H_2O (KOH: $x = 1.8 \times 10^{-4}$); ●, sample B, DXL·16.97H_2O ($x = 1.8 \times 10^{-3}$).

hydrates [14, 15]. This means that the reorientational motions of the water molecules in DXL hydrates doped with KOH are similar to those of other KOH-doped hydrates previously studied. In spite of a similar relaxational property, the ordering transition did not occur in the present samples. It is noteworthy that the activation enthalpy of sample B is close to that of sample A even though the KOH concentration of sample B was ten times higher than that of sample A. We assume that the solubility limit of KOH into the hydrate crystal is around $x = 1.8 \times 10^{-4}$ and so most of the extra KOH in sample B was excluded from the hydrate. This conjecture is supported by the existence of the eutectic melting at 216 K in sample B probably between the DXL clathrate hydrate and a stoichiometric KOH hydrate whose composition is unknown.

3.3. *Phase transition in DXL–THF mixed hydrate*

Fig. 4 shows the DTA curves of the 6 samples of $DXL_{1-x}THF_x$ mixed hydrates. The sensitivity of the measurements for the samples of $x \leq 0.8$ was 2.5 times larger than that for the samples of $x > 0.8$. In the THF hydrate ($x = 1$), a sharp endothermic peak due to the ordering transition involving both the guest and host molecules appeared at 62 K as reported [9, 12]. As the concentration of DXL increased, the transition temperature decreased and the peak shape became broader. The transition peak was not observed in the sample of $x = 0.5$.

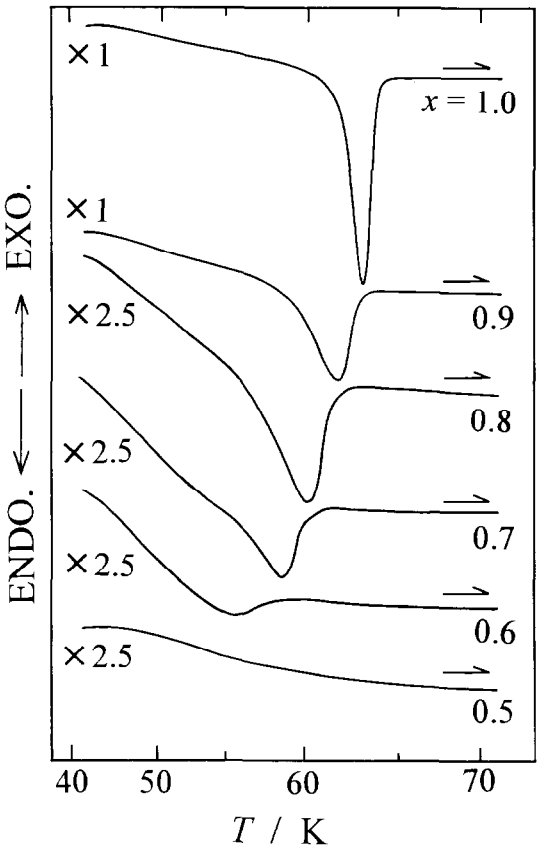

Fig. 4. DTA curves of 1,3-dioxolane and tetrahydrofuran mixed hydrates ($DXL_{1-x}THF_x \cdot 16.5H_2O$) doped with KOH ($x = 1.8 \times 10^{-4}$).

Since it was difficult to determine the transition temperatures because of the broadening of the peak, the peak top and the rising temperatures were plotted as a function of x as shown in Fig. 5. From the extrapolations shown by the broken lines (2nd order polynomial of x), the transition temperature at $x = 0$ was determined to be between 20 and 44 K. If the transition temperature is taken as the center of this region (37 K), it is much lower than the glass transition temperature (44 K).

The relative peak areas to that of the THF hydrate ($x = 1$) were plotted as a function of x, the open circles in Fig. 6. The effect of the sensitivity of the Cr–Co thermocouple was corrected. The error bars are due to the uncertainty of the baseline. The peak area decreases almost linearly with decreasing x and vanishes at about $x = 0.5$. To investigate the reason for this, the sample with $x = 0.6$ was annealed

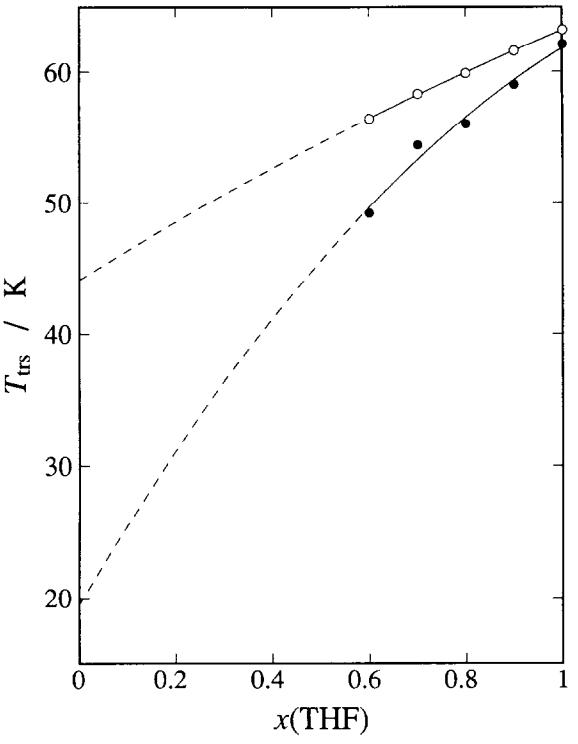

Fig. 5. Composition dependence of the transition temperature of ($DXL_{1-x}THF_x \cdot 16.5H_2O$) doped with KOH ($x = 1.8 \times 10^{-4}$): ○, peak temperatures; ●, rising temperatures.

at 46 K for 1 h and then a DTA curve was recorded with the same conditions as the first run. The peak area thus obtained (solid circles in Fig. 6) was increased by about 30% of those of the first run. This result indicates that the decrease in peak area with decrease in x was not due to the equilibrium property of the hydrates but to the kinetics of the transition, i.e. the lower the THF concentration x, the slower the transition rate.

Thus, DTA of the DXL–THF mixed hydrate clarified the reason for the absence of the ordering transition in the DXL hydrate: the transition temperature of the DXL hydrate is lower than the glass transition temperature of the water reorientational motion. Another significant result of the present study is that the transition temperatures of the clathrate hydrates are quite sensitive to the guest molecules. The guest property governing the transition temperature is not simply the dipole moment nor the maximum van der Waals diameter because those of THF and DXL are similar. A structural study in the low-temperature phase is desirable for clarification of the transition mechanism.

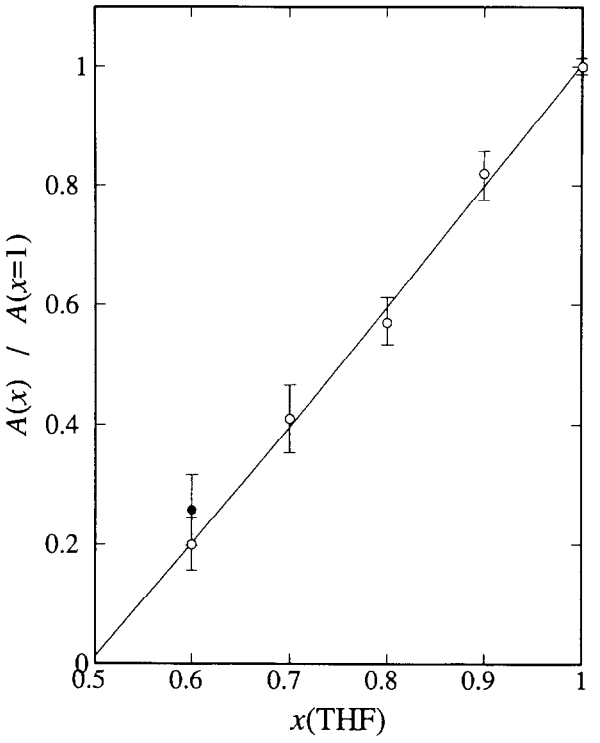

Fig. 6. Composition dependence of the relative peak area of the transition of ($DXL_{1-x}THF_x \cdot 16.5H_2O$) doped with KOH ($x = 1.8 \times 10^{-4}$): ○, normal runs; ●, run after annealing at 46 K for 1 h.

Appendix

The standard thermodynamics functions

The molar heat capacities, enthalpies, entropies and Giauque functions of 1,3-dioxolane clathrate hydrate ($DXL \cdot 16.95H_2O$) doped with KOH ($x = 1.8 \times 10^{-4}$) were calculated from the smoothed heat capacity data and are summarized in Table 2. The heat capacity was extrapolated down to 0 K using the polynomial

$$C_p/(\mathrm{J\,K^{-1}\,mol^{-1}}) = 1.8798 \times 10^{-2}(T/\mathrm{K})^3 - 4.0197 \times 10^{-5}(T/\mathrm{K})^5 + 3.4636 \times 10^{-8}(T/\mathrm{K})^7$$

where the three coefficients were determined by the least-squares fitting to the heat capacity data in the temperature range 13–20 K.

Table 2
Molar thermodynamic functions of 1,3-dioxolane clathrate hydrate (DXL·16.95H_2O) doped with KOH ($x = 1.8 \times 10^{-4}$) ($M = 379.38\ g\ mol^{-1}$, $R = 8.31451\ J\ K^{-1}\ mol^{-1}$, $\Phi_m^\circ = \Delta_0^T S_m^\circ - \Delta_0^T H_m^\circ/T$)

T/K	$C_{p,m}^\circ/R$	$\Delta_0^T H_m^\circ/RT$	$\Delta_0^T S_m^\circ/R$	Φ_m°/R
10	1.819	0.4899	0.6630	0.1731
20	7.948	2.610	3.697	1.087
30	14.67	5.521	8.205	2.684
40	20.59	8.564	13.25	4.690
50	25.82	11.50	18.42	6.919
50	29.36	11.51	18.43	6.919
60	31.79	14.69	24.00	9.309
70	34.05	17.30	29.07	11.78
80	36.28	19.53	33.76	14.23
90	38.49	21.51	38.16	16.65
100	40.70	23.32	42.33	19.01
110	42.93	25.00	46.32	21.31
120	45.18	26.59	50.15	23.56
130	47.48	28.11	53.86	25.75
140	49.83	29.58	57.46	27.88
150	52.24	31.01	60.98	29.97
160	54.73	32.41	64.43	32.02
170	57.28	33.80	67.82	34.03
180	59.91	35.18	71.17	36.00
190	62.61	36.55	74.48	37.94
200	65.39	37.92	77.77	39.85
210	68.27	39.30	81.03	41.73
220	71.29	40.68	84.27	43.59
230	74.51	42.08	87.51	45.43
240	78.04	43.50	90.75	47.25
250	82.03	44.96	94.02	49.05
260	89.81	46.51	97.36	50.85
270	537.8	49.66	101.4	51.75
Congruent melting at 270.5 K				
273.15	171.1	66.98	119.5	52.49
280	171.5	69.54	123.7	54.18
290	172.4	73.07	129.8	56.68
298.15	172.9	75.79	134.5	58.75
300	173.1	76.39	135.6	59.22

References

[1] J.L. Atwood, J.E.D. Davies and D.D. MacNicol (Eds.), Inclusion Compounds, Academic Press, London, 1984.
[2] D.W. Davidson, Water: A Comprehensive Treatise, Vol. 2, Chap. 3, Plenum Press, New York, 1973.
[3] B. Berecz and M. Balla-Achs, Gas Hydrates, Studies in Inorganic Chemistry 4, Elsevier, Amsterdam, 1983.

[4] O. Yamamuro and H. Suga, J. Therm. Anal., 35 (1989) 2025.
[5] G.A. Jeffrey and R.K. McMullan., Prog. Inorg. Chem., 8 (1967) 43.
[6] O. Yamamuro, Y.P. Handa, M. Oguni and H. Suga, J. Incl. Phenom., 8 (1990) 45.
[7] Y.P. Handa, Can. J. Chem., 63 (1985) 68.
[8] N. Kuratomi, O. Yamamuro, T. Matsuo and H. Suga, J. Therm. Anal., 38 (1992) 1847.
[9] O. Yamamuro, M. Oguni, T. Matsuo and H. Suga, J. Phys. Chem. Solids, 49 (1988) 425.
[10] N. Kuratomi, O. Yamamuro, T. Matsuo and H. Suga, J. Chem. Thermodyn., 23 (1991) 485.
[11] S.R. Gough, S.K. Garg and D.W. Davidson, Chem. Phys., 3 (1973) 239.
[12] O. Yamamuro, M. Oguni, T. Matsuo and H. Suga, Solid State Commun., 62 (1987) 289.
[13] O. Yamamuro, N. Kuratomi, T. Matsuo and H. Suga, Solid State Commun., 73 (1990) 317.
[14] O. Yamamuro, T. Matsuo and H. Suga, J. Incl. Phenom., 8 (1990) 33.
[15] O. Yamamuro, N. Kuratomi, T. Matsuo and H. Suga, J. Phys. Chem. Solids, 54 (1993) 229.
[16] Y.P. Handa, J. Chem. Thermodyn., 17 (1985) 201.
[17] Y.P. Handa, J. Chem. Thermodyn., 16 (1984) 623.
[18] K. Moriya, T. Matsuo and H. Suga, J. Chem. Thermodyn., 14 (1982) 1143.
[19] R.N. Goldberg and R.D. Weir, Pure Appl. Chem., 64 (1992) 1545.
[20] M. Oguni, N. Okamoto, O. Yamamuro, T. Matsuo and H. Suga, Thermochim. Acta, 121 (1987) 323.